

Direct geoelectrical evidence of mass transfer at the laboratory scale

Ryan D. Swanson,¹ Kamini Singha,² Frederick D. Day-Lewis,³ Andrew Binley,⁴ Kristina Keating,⁵ and Roy Haggerty⁶

Received 21 May 2012; revised 7 September 2012; accepted 13 September 2012; published 25 October 2012.

[1] Previous field-scale experimental data and numerical modeling suggest that the dual-domain mass transfer (DDMT) of electrolytic tracers has an observable geoelectrical signature. Here we present controlled laboratory experiments confirming the electrical signature of DDMT and demonstrate the use of time-lapse electrical measurements in conjunction with concentration measurements to estimate the parameters controlling DDMT, i.e., the mobile and immobile porosity and rate at which solute exchanges between mobile and immobile domains. We conducted column tracer tests on unconsolidated quartz sand and a material with a high secondary porosity: the zeolite clinoptilolite. During NaCl tracer tests we collected nearly colocated bulk direct-current electrical conductivity (σ_b) and fluid conductivity (σ_f) measurements. Our results for the zeolite show (1) extensive tailing and (2) a hysteretic relation between σ_f and σ_b , thus providing evidence of mass transfer not observed within the quartz sand. To identify best-fit parameters and evaluate parameter sensitivity, we performed over 2700 simulations of σ_f , varying the immobile and mobile domain and mass transfer rate. We emphasized the fit to late-time tailing by minimizing the Box-Cox power transformed root-mean square error between the observed and simulated σ_f . Low-field proton nuclear magnetic resonance (NMR) measurements provide an independent quantification of the volumes of the mobile and immobile domains. The best-fit parameters based on σ_f match the NMR measurements of the immobile and mobile domain porosities and provide the first direct electrical evidence for DDMT. Our results underscore the potential of using electrical measurements for DDMT parameter inference.

Citation: Swanson, R. D., K. Singha, F. D. Day-Lewis, A. Binley, K. Keating, and R. Haggerty (2012), Direct geoelectrical evidence of mass transfer at the laboratory scale, *Water Resour. Res.*, 48, W10543, doi:10.1029/2012WR012431.

1. Introduction

[2] Tracer experiments in saturated porous media commonly show anomalous, non-Fickian tracer transport, characterized by (1) early breakthroughs of tracer; (2) over- and under-estimates of mass at early and late times,

respectively; (3) tailing, or a gradual decrease in concentration through time, resulting in elevated concentration levels at late times; and (4) contaminant storage and rebound, or the apparent increase in concentration some time after sampling. These characteristics are often observed through pumping and sampling of the mobile pore space, and none of these transport characteristics can be explained with an advective-dispersive model (ADM), except perhaps when exhaustive data are available [e.g., Adams and Gelhar, 1992; Garré et al., 2010; Huang et al., 1995; Moroni et al., 2007; Sidle et al., 1998; Silliman et al., 1987]. Recent laboratory-scale work shows that even with extensive knowledge of the velocity field, non-Fickian transport may be present and cannot be accounted for by unknown, smaller scale heterogeneities [Major et al., 2011]. Understanding the cause and effects of this anomalous transport is particularly important for groundwater management, including groundwater remediation [Harvey et al., 1994] and aquifer storage and recovery operations [Culkin et al., 2008].

[3] Other models besides the ADM can provide a better fit to concentration histories and account for non-Fickian behavior. One simple conceptual model is the dual-domain mass transfer (DDMT) model, which partitions the unresolved heterogeneity into a mobile and immobile porosity

¹Department of Geology and Geologic Engineering, Hydrologic Science and Engineering, Colorado School of Mines, Golden, Colorado, USA.

²Department of Geology and Geological Engineering and Department of Civil and Environmental Engineering, Hydrologic Science and Engineering, Colorado School of Mines, Golden, Colorado, USA.

³Office of Groundwater, Branch of Geophysics, U.S. Geological Survey, Storrs, Connecticut, USA.

⁴Lancaster Environment Centre, Lancaster University, Lancaster, UK.

⁵Department of Earth and Environmental Sciences, Rutgers, State University of New Jersey, New Brunswick, New Jersey, USA.

⁶College of Earth, Ocean and Atmospheric Sciences, Oregon State University, Corvallis, Oregon, USA.

Corresponding author: R. D. Swanson, Department of Geology and Geologic Engineering, Hydrologic Science and Engineering, Colorado School of Mines, 214 Berthoud Hall, Golden, CO 80401, USA. (ryswans@mymail.mines.edu)

(or domain) [Coats and Smith, 1964; van Genuchten and Wierenga, 1976]. In this conceptual model, advection and dispersion are limited to the mobile domain, and mass is temporarily stored in the immobile domain. Mass exchange between the domains is governed by a first-order single rate of exchange, and temporary storage in the immobile domain is a potential source for tailing. For example, at early time, following a pulse injection of a saline tracer into a freshwater environment, the immobile domain would be relatively fresh and act as a solute sink for the mobile domain, which is inundated by the tracer. At late time, when the mobile domain is relatively clean after the majority of the plume has transported out of that part of the system, solute would be slowly released from the immobile domain. This slow, extended release is the source of tailing and contaminant storage and rebound in the DDMT model. More complex models describing anomalous transport exist, including fractional advection-dispersion equation models that are nonlocal in space [Benson *et al.*, 2000; Meerschaert *et al.*, 1999] and nonlocal in time, including the continuous time random walk models [Berkowitz *et al.*, 2002, 2006]. The appeal of DDMT is its simplicity, which may be too simple for many systems; distributions of mass transfer rates and length scales are more likely than one rate, and this process can be explained using a multirate mass transfer model [Carrera *et al.*, 1998; Haggerty and Gorelick, 1995; Haggerty *et al.*, 2000]. The DDMT model may not be able to match concentration histories as well as these more complex models, but we chose this model for its simplicity of interpretation when electrical measurements are used in conjunction with standard fluid samples.

[4] Despite the success of nonlocal models at matching concentration histories, the parameters are difficult to measure directly and lack experimental verification, although some limited previous work has shown that these values may be correlated to the statistics of the hydraulic conductivity field [Benson *et al.*, 2001; Willmann *et al.*, 2008], facies distributions [Zhang *et al.*, 2007], or fracture length scale [e.g., Reeves *et al.*, 2008]. The main limitation of many nonlocal models is the “weak predictability of the model and its main parameters” [Zhang *et al.*, 2009]; in other words, the physical meaning of many of the model parameters is difficult to interpret and relate to the geologic properties of the system [e.g., Willmann *et al.*, 2008]. For a DDMT model, which splits the earth system into two domains, point-source fluid samples are drawn preferentially from the mobile domain and can therefore inform only on that space, while sampling from the immobile domain is commonly impractical and expensive as it requires coring and destructive testing. The unknown parameters of the DDMT model are often model-calibrated a posteriori by maximizing the match between observations and model simulations—minimizing an objective function—but this and other methods of parameter calibration lack physical confirmation.

[5] Here we seek to (1) experimentally observe the geoelectric signature of mass transfer at the laboratory scale through tracer tests on well-characterized materials and (2) demonstrate the estimation of DDMT parameters from experimental data and compare these to model-calibrated parameters. Direct-current geophysical methods should be

sensitive to both the immobile and mobile domains through measurements of bulk conductivity (σ_b , $\mu\text{S}/\text{cm}$), providing a unique advantage over standard sampling. We demonstrate, for the first time, the synthesis of point-scale fluid samples of fluid conductivity (σ_f , $\mu\text{S}/\text{cm}$) and electrical geophysical data to directly quantify anomalous mass transfer behavior in situ, and provide controlled laboratory evidence to show that the σ_b - σ_f hysteresis observed in field data [Singha *et al.*, 2007] is a function of mass transfer between mobile and immobile domains. We collected electrical resistivity measurements made on controlled media (i.e., quartz sand and zeolites) in column experiments to isolate the effect of mass transfer from other factors such as heterogeneity or difference in support scale [Wheaton and Singha, 2010]. Low-field nuclear magnetic resonance (NMR) measurements are used to corroborate the pore size distribution and link the best-fit estimates of mobile and immobile porosity obtained from time-lapse fluid sample measurements.

2. Methods

[6] Laboratory-scale tracer tests were performed in columns packed with (1) well-sorted, well-rounded, spherical Accusand sand grains of 0.8 to 1.7 mm in diameter (Accusand, Unimin Corporation, Minnesota; Figures 1a–1c); and (2) angular, 2.4 to 4.8 mm diameter grains of the zeolite clinoptilolite (Zeox Corporation, Calgary, Alberta; Figures 1d–1f). We selected sand as a control and zeolite for its unique internal porosity network consisting of a distribution of pore sizes, and this zeolite has been shown to have a large interparticle porosity (32.2%) and bed porosity (52%–58%) [Kowalczyk *et al.*, 2006; Sprynskyy *et al.*, 2010]. Tracer tests were conducted in 22.3 cm long and 5.08 cm diameter polyvinyl chloride (PVC) columns, which were wet packed by incrementally adding saturated material, followed by successive tapping on the sides of the column and pressing down on the material with a pestle as detailed by Oliviera *et al.* [1996].

2.1. Laboratory-Scale Tracer Experiments

[7] We selected sodium chloride (NaCl) as our ionic tracer. Filter paper was placed near the inlet and outlet of each column to evenly distribute the NaCl solution and prevent solid particles from leaving the column. A peristaltic pump was used to inject fluid from the bottom of the column upward, and σ_f was measured by a flow-through probe placed at the outlet of the column (see Figure 2a). At 1 mL min⁻¹, a 0.4 g L⁻¹ ($\sigma_f \sim 800 \mu\text{S}/\text{cm}$) NaCl solution was injected continuously before the start of the experiment to ensure equilibrium between the mobile and immobile domains, followed by a 1.5 L, 25 h long pulse of 1.15 g L⁻¹ ($\sigma_f \sim 2300 \mu\text{S}/\text{cm}$) tracer and then back to the initial 0.4 g L⁻¹ solution. Multiple pore volumes of tracer were injected to allow the mobile and immobile domains to reach equilibrium, indicated when σ_b and σ_f no longer vary in time. Flow rates were measured continuously and fluid samples were collected periodically for ion chromatography analysis of chloride concentration.

2.2. Electrical Resistivity Measurements

[8] Seven sets of four stainless-steel potential electrodes were spaced 2.5 cm apart vertically with radial symmetry

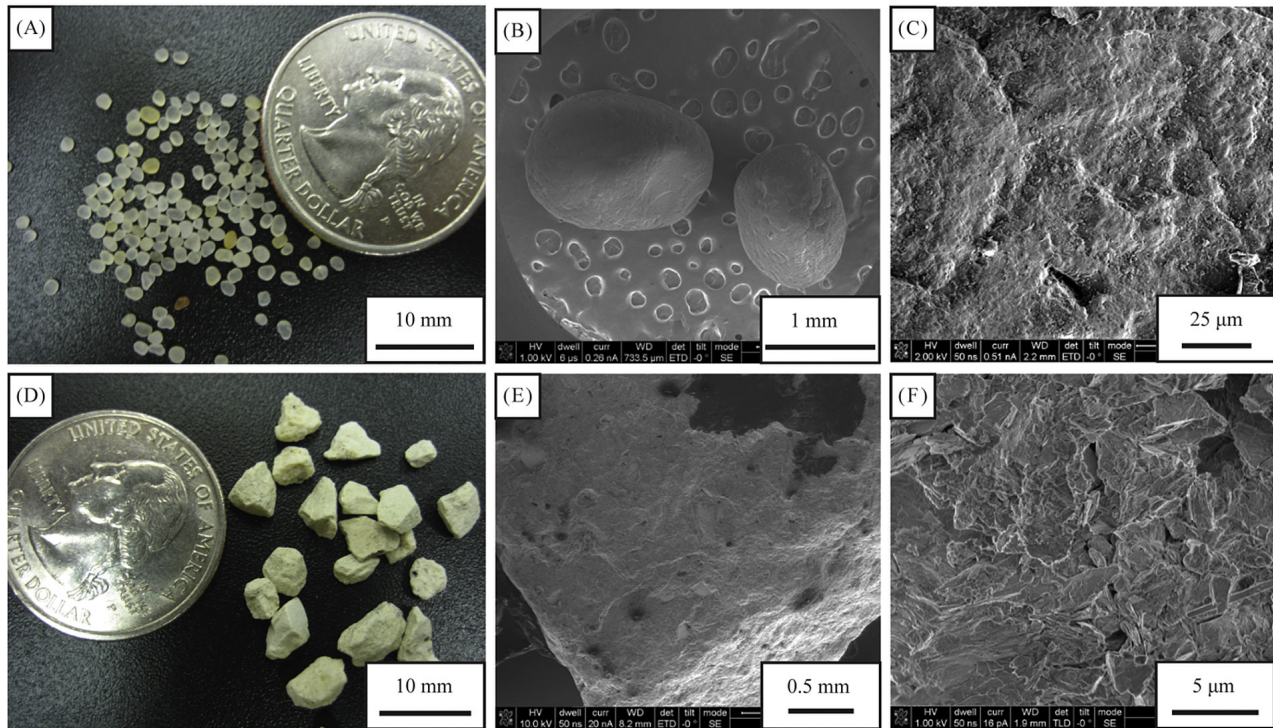


Figure 1. (a) Grains of sand consisting of over 99% silica. (b and c) SEM images of the sand grains reveal little surface topography. (d) Grains of the zeolite clinoptilolite. (e and f) SEM images of the zeolite grains show a textured surface with surface topography.

around the column at 90° from one another (see Figure 2). Brass wire mesh current electrodes were placed in the end caps of the column. The resistance R (Ω) of each adjacent electrode pair was calculated from Ohm's law by

measuring the voltage drop for a known applied current using a 10-channel resistivity meter (Syscal Pro, IRIS Instruments, France) with an accessory for low-current measurements at this small scale. Then, σ_b was determined by the inverse of the product of R and a geometric factor K (m), a function of the geometric position of current and potential electrodes:

$$\sigma_b = (RK)^{-1}. \quad (1)$$

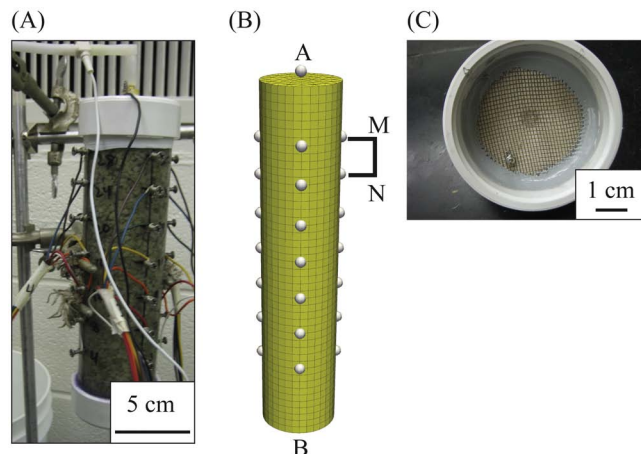


Figure 2. (a) An example column used for the tracer test showing the location of the electrodes and the fluid conductivity probe at the outlet. (b) A schematic showing potential electrodes (M,N) spaced evenly every 2.5 cm and current electrodes (A,B) at the top and bottom of the column. The current electrode is (c) a brass mesh rather than a point, which is placed in the end caps of the column.

The geometric factor for each vertically adjacent electrode pair was experimentally determined by filling the column with a solution of known σ_f with no solids present, so σ_f and σ_b are equal, and then dividing the known σ_f by the measured resistance.

[9] Electrical measurements were collected at a rate of 75 measurements every minute. For the nearly colocated measurements of σ_b and σ_f , only the vertical potential pair nearest the σ_f probe was used for analysis. We corrected for the time lag between the σ_b and σ_f measurement locations using the estimated pore water velocity and distance between measurement locations. The homogeneously packed system can be treated as a one-dimensional (1-D) system, so we use the resistivity measured between potential pairs as a representative value located between the two pairs. Colocated measurements at the electrode pairs nearest the outlet were collected at a rate of 3 measurements every minute, and this temporal resolution is sufficient to adequately measure mass transfer [Day-Lewis and Singha, 2008].

2.3. Dual Domain Mass Transfer Model

[10] The simplest, 1-D form of the DDMT model can be mathematically described using two equations [van Genuchten and Wierenga, 1976]:

$$\theta_m \frac{\partial C_m}{\partial t} + \theta_{im} \frac{\partial C_{im}}{\partial t} = \theta_m D \frac{\partial^2 C_m}{\partial x^2} - \theta_m v \frac{\partial C_m}{\partial x}, \quad (2a)$$

$$\theta_{im} \frac{\partial C_{im}}{\partial t} = \alpha (C_m - C_{im}), \quad (2b)$$

where θ_m and θ_{im} are the mobile and immobile porosities (–), respectively; C_m and C_{im} are the concentration of the mobile and immobile domains (kg m^{-3}), respectively; D is the spatially constant dispersion coefficient ($\text{m}^2 \text{s}^{-1}$); v is the spatially constant average pore water velocity (m s^{-1}); and α is the mass transfer rate coefficient (s^{-1}). The mass transfer rate can be physically conceptualized as diffusion over a length scale squared, where the length scale is the path solutes diffuse into and out of the immobile domain. A length scale can be calculated for a given mass transfer rate and coefficient for diffusion. The rate of exchange of mass in and out of the immobile pore space depends solely on the difference in concentration between the two domains and the mass transfer rate.

[11] Certain conditions must be met in order for mass transfer to be observed in the mobile breakthrough curve signal. The magnitude of mass transfer depends on the Damköhler number DaI , a dimensionless number that describes the relative importance of mass transfer to advection [Bahr and Rubin, 1987]:

$$DaI = \frac{\alpha \left(1 + \frac{\theta_{im}}{\theta_m}\right) L}{v}, \quad (3)$$

where L (m) is the observation length away from the initial source of mass where samples are collected. When $DaI \ll 1$, mass transfer is slow relative to advection and advection dominates. When $DaI \gg 1$, mass exchanges rapidly (relative to advection) between the domains, which are approximately in equilibrium. As a result, tailing and anomalous transport are not observed. When $DaI \sim 1$, both advection and mass transfer are important and anomalous behavior is observed. The average pore water velocity is an experimental variable directly related to the flow rate, which we adjust to achieve a DaI number favorable to investigating anomalous behavior.

2.4. 1-D Numerical Simulations

[12] We used the finite element solver COMSOL Multiphysics to simulate solute transport using the Earth Sciences Solute Transport software package. Initial and boundary conditions are based on the laboratory setup with time-varying, specified concentration Dirichlet boundary conditions at the inlet and an advective flux boundary at the outlet. We assumed radial symmetry to reduce the transport simulations of our 22.3 cm column to a 1-D model consisting of 60 equally spaced, 0.38 cm elements. These simulations were performed within a DDMT framework, assuming a first-order mass transfer rate for exchange of solute between the mobile and immobile domain as shown in equations (2a) and (2b). Both advection and diffusion were

set to zero for the immobile domains, whereas both exist in the mobile pore space. Diffusion is equal to $1.25 \times 10^{-9} \text{ m}^2 \text{ s}^{-1}$ in the mobile pore space. In the model described here diffusion only accounts for the diffusion of solutes associated with transport (i.e., movement along the column due to concentration gradients) and does not drive mass transfer (i.e., diffusion in and out of immobile pore space). The diffusion in and out of immobile pores space is handled by the mass transfer rate α in equation (2b). Dispersivity is usually set at an order of magnitude below the distance to the point of observation, but a visual inspection of the breakthrough curve revealed that this dispersivity value was too high for all experiments, likely due to the homogenous nature of the packed columns. Rather than vary the dispersivity for each experiment as an additional parameter, the dispersivity was set to 0.1 cm for all simulations based on matching the σ_f in the sand experiment to ADM model simulations and set for zeolite experiments.

[13] Parametric sweeps were performed by adjusting DDMT parameters (mobile and immobile porosities and the mass transfer rate) and holding all variables constant. The mass transfer rate was evaluated from 10^{-3} to 10^{-8} s^{-1} with increments increasing by an order of magnitude. The mobile and immobile porosities were evaluated over the interval from 1% to 65% at increments of 2.7%. Simulations with total porosity less than 15% or greater than 85% were not considered because they were unrealistic. The total number of simulations considered was 2742. Concentration was converted to σ_f using the linear relation defined by Keller and Frischknecht [1966]. Although running multiple forward models rather than an inverse approach is more computationally expensive, this method allows for a visual evaluation of the sensitivity for each parameter.

2.5. Linking Electrical Methods to Anomalous Transport

[14] The most commonly used relation between σ_b and σ_f , ignoring surface conductivity, is the empirical Archie's law [Archie, 1942]:

$$\sigma_b = a \sigma_f \theta^m, \quad (4)$$

where a is a dimensionless fitting parameter representing tortuosity (–) and m is the cementation factor (–). Archie's law does not account for mass transfer into immobile domains and predicts a strictly linear relation between σ_b and σ_f . However, hysteresis between σ_b and σ_f has been observed in both field and synthetic numerical modeling experiments and has been suggested to be a function of the unequal distribution of solutes between immobile and mobile domains [Day-Lewis and Singha, 2008; Singha et al., 2007]. In a dual-domain system, Archie's law is not appropriate without modification to include multiple domains since both the immobile and mobile components contribute to σ_b .

2.6. Material Characterization

[15] Understanding the physical makeup of our materials is fundamental to predicting and interpreting the solute transport behavior in our columns, and confirming the geophysical signatures we measured. The materials used in this study were characterized using X-ray diffraction (XRD)

and scanning electron microscopy (SEM). XRD analysis was used primarily to detect the presence of clays. SEM images were used to identify surface features on the sub-micron scale that may contribute to immobile pore space. Additionally, the water content in the saturated samples was determined gravimetrically and taken to be equivalent to the total porosity.

2.7. Nuclear Magnetic Resonance

[16] Independent methods for characterizing the mobile and immobile parameters remain elusive but paramount to connecting best-fit calculated parameters to a physical representation of the pore space. We used low-field proton NMR measurements to partition the total porosity into an immobile and mobile porosity based on the distribution of transverse relaxation times.

[17] The measured NMR signal $I(t)$ is described by a multiexponential decay

$$I(t) = I_0 \sum f_i e^{-t/T_{2i}}, \quad (5)$$

where I_0 is the initial signal magnitude. Using an instrument specific calibration factor, I_0 can be converted into the total volume of water measured in the NMR experiment. The subscript i in equation (5) represents each pore environment and f_i is the fraction of protons relaxing with a relaxation time of T_{2i} . The values of f_i versus T_{2i} are often plotted to show the distribution of relaxation times. In the case of fast diffusion, which assumes that all protons travel to and relax at the solid surface in the time interval of the NMR experiment, the i th relaxation time value is given by [Brownstein and Tarr, 1979; Senturia and Robinson, 1970]

$$\frac{1}{T_{2i}} \sim \frac{\rho_{2i}}{a_i} \quad (6)$$

where a_i is the characteristic length scale of the i th water-filled pore, typically described by the inverse of the surface-area-to-volume ratio of the corresponding pore, and ρ_{2i} is the surface relaxivity or the ability of the surface to enhance relaxation. For porous material with uniform ρ_{2i} , e.g., clean sand, the T_2 distribution can be used to represent the pore size distribution. Previous studies have verified this relation for a range of water-saturated porous material including: sandstone and carbonate cores [Arns, 2004; Straley et al., 1997]; silica gels [Valckenborg et al., 2001]; fused glass beads [Straley et al., 1987]; and unconsolidated sand and glass beads [Bird et al., 2005; Hinedi et al., 1993]. Furthermore, an early study by Timur [1969] showed that θ_{im} can be estimated from $\theta_{im} = \sum_{T_{2i} < T_{2cutoff}} f_i$, where $T_{2cutoff}$ is an empirically defined cutoff time; similarly, θ_m can be estimated from $\theta_m = \sum_{T_{2i} > T_{2cutoff}} f_i$. In sandstone cores, a cutoff time of 33 ms is commonly used to accurately determine immobile and mobile porosities [Allen et al., 2000; Timur, 1969].

[18] To create samples for NMR measurement, the sand and zeolites were separately packed into Teflon containers using the same methods as described in section 2. The media packed sample holders were saturated with tap water under a vacuum as described by Keating and Knight [2010]

and covered with parafilm to prevent the evaporation of water from the sample. NMR relaxation data were collected with a 2 MHz Rock Core Analyzer (Magritek Ltd) using a CPMG (Carr-Purcell-Meiboom-Gill) pulse sequence. For each sample, 40 data points were obtained at each echo, and 50,000 echoes were collected with an echo spacing of 300 μ s. Each set of measurements was stacked 32 times with a delay time of 10 s. The T_2 distribution was determined by applying a non-negative least squares inversion with Tikhonov regularization to a logarithmically subsampled set of the NMR data [Whittall et al., 1991]. The regularization parameter was selected such that each datum was misfit by approximately one standard deviation.

[19] The distribution of relaxation times can be used to approximate the total mobile and immobile porosity domains and provides an independent estimate that can be compared to the values determined using the curve-fitting methods. The total porosity can also be estimated from the NMR data for each sample by measuring the initial signal amplitude, converting to the total water volume using an instrument-specific calibration factor, and then converting the total water volume estimate to total porosity by adjusting for the known total volume of the sample holder. NMR measurements were repeated three times, and the total, immobile, and mobile porosities were calculated separately for each sample. The numbers reported are the mean of each of these materials for the three samples and the error is the standard deviation.

2.8. Estimating Best-Fit Parameters

[20] Best-fit DDMT parameters (θ_m , θ_{im} , and α) are often determined through numerical simulations by minimizing an objective function. One method includes minimizing the root-mean square error (RMSE) between observed and measured σ_f , defined as

$$RMSE = \sqrt{\frac{1}{n} \sum_{t=1}^n (\sigma_{f,s,t} - \sigma_{f,m,t})^2}, \quad (7)$$

where n is the number of observations and $\sigma_{f,s,t}$ and $\sigma_{f,m,t}$ are the simulated and measured σ_f , respectively, at time step t . As a pulse of tracer moves and is sampled, the rising and falling limbs of the breakthrough curve rise and fall rapidly. Small changes in the mobile porosity can have a large effect on the arrival of tracer, and if the timing is slightly off between simulated and measured σ_f during this portion of the tracer test, the difference and RMSE will be high. Minimizing the RMSE will preferentially minimize these times. However, we are particularly interested in the late-time tailing, so we use the Box-Cox power transform on both the measured and simulated σ_f and use the transformed values in our estimate of the TRMSE (transformed root-mean square error) [Box and Cox, 1964]:

$$Z = \frac{(1 + \sigma_f)^\lambda - 1}{\lambda}, \quad (8)$$

$$TRMSE = \sqrt{\frac{1}{n} \sum_{t=1}^n (Z_{s,t} - Z_{m,t})^2}, \quad (9)$$

where λ is the transformation parameter and $Z_{s,t}$ and $Z_{m,t}$ are the transformed simulated and measured σ_f , respectively.

We chose a λ value of 0.3 because it emphasizes the smaller measured values observed at late times and has been previously used to minimize the late time of hydrographs, and we extend this use here to emphasize the fit to the late-time tailing behavior [Kollat *et al.*, 2012; Misirli *et al.*, 2003; van Werkhoven *et al.*, 2009]. The minimum TRMSE corresponds to the best-fit DDMT parameters including the mobile and immobile porosities and the mass transfer rate that emphasize the fit to late-time tailing.

3. Results

3.1. Accusand

[21] XRD analysis shows nearly pure (>99%) quartz grains, free of clay. SEM images show smooth grains with little surface topography (Figures 1b and 1c). The gravimetric method of calculating porosity indicates a total porosity of 34%. NMR results show multiple peaks in the distribution of relaxation times (Figure 3a). Using a 33 ms cutoff [Allen *et al.*, 2000; Timur, 1969], the majority of the total porosity ($31.7 \pm 0.3\%$) determined from NMR methods is mobile ($31 \pm 0.3\%$), with the remaining $0.7 \pm 0.1\%$ of the total porosity potentially serving as immobile pore space. The porosity calculations and best-fit parameters are listed in Table 1.

[22] In the well-sorted sand column, σ_f and σ_b behave as predicted by Archie's law, with negligible hysteresis (Figures 4a and 4b). The measured σ_f is consistent with ion chromatography analyses of collected fluid samples, and the total mass recovery is 99%, as calculated from temporal moments of σ_f . Assuming advective-dispersive transport, the mean arrival time indicates a porosity of 33%. Parametric sweeps performed in COMSOL indicate a mobile porosity of 33% (shown only for the best-fit mass transfer rate; Figure 4c). The best-fit immobile porosity is 1% and mass transfer rate is 10^{-5} s^{-1} determined from minimizing misfit between modeled and observed σ_f .

3.2. Zeolite

[23] XRD analysis of the zeolite indicates a sample dominated by clinoptilolite with minor amounts of quartz and no strong indicators of any clay phases. SEM images

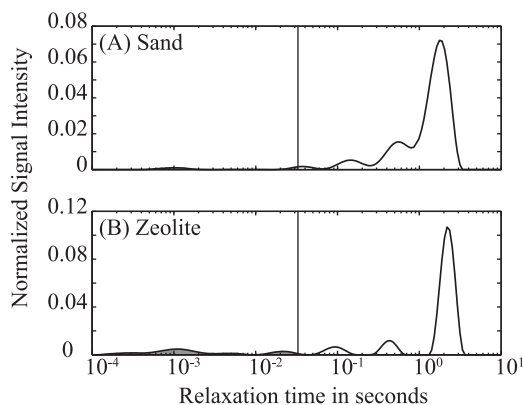


Figure 3. The relaxation time distributions for (a) sand and (b) zeolite show multiple peaks, representative of different pore sizes. Cutoff times separate the total estimated porosity into either mobile or immobile porosity.

Table 1. Estimated and Best-Fit Parameters

Material	Parameters	Method		
		Gravimetric	TRMSE	NMR
Sand	Total Porosity	0.34	0.34	0.32
	Mobile Porosity	–	0.33	0.31
	Immobile Porosity	–	0.01	0.01
	Mass Transfer Rate (s^{-1})	–	10^{-5}	–
	<i>DaI</i>	–	0.1	–
Zeolite	Total Porosity	0.54	0.66	0.50
	Mobile Porosity	–	0.46	0.43
	Immobile Porosity	–	0.2	0.07
	Mass Transfer Rate (s^{-1})	–	10^{-5}	–
	<i>DaI</i>	–	0.2	–

of the zeolite (Figures 1e and 1f) show a rough surface topography dominated by layered sheets of varying relief with minor, smaller regions composed of faceted crystals. The gravimetric method of calculating porosity indicates a value of 54%. The NMR results for the zeolite (Figure 3b) show multiple peaks in the relaxation time distribution. Using the same 33 ms cutoff for the zeolite as the sand, the mobile and immobile porosities determined from this method are $43 \pm 1\%$ and $7.7 \pm 0.3\%$, respectively, and the total porosity is $50.3 \pm 0.9\%$.

[24] The zeolite column shows significant tailing in σ_f and σ_b (Figure 5a). The relation between σ_f and σ_b varies in time, resulting in hysteresis as the σ_b lags behind σ_f as solutes are trapped and released from the immobile domain (Figure 5b). The ratio between σ_f and σ_b could be described as an “apparent formation factor” that changes through time, but an unmodified Archie's law does not apply for a mobile-immobile system. We find a best-fit mobile porosity of 46%, immobile porosity of 20%, and mass transfer rate of 10^{-5} s^{-1} based on matching simulated and observed σ_f (shown only for the best-fit mass transfer rate; Figure 5c). The corresponding length scale of mass transfer is 2.4 cm, assuming diffusion in and out of cylinders [Haggerty and Gorelick, 1995], which is within an order of magnitude of the grain size (2.4 to 4.8 mm). Temporal moment analysis of the σ_f indicates that 100% of the mass was recovered.

4. Discussion

4.1. Accusand

[25] XRD analysis shows nearly pure silica grains of sand, whereas SEM images reveal that the sand grains do not appear to have any major internal porosity that could serve as immobile domains to trap, store, and release solutes. The modeled best-fit mobile and immobile porosities (33% and 1%, respectively) are consistent with the weight-based measurement of 34%. NMR measurements estimate a mobile porosity of 31% and little immobile porosity (0.7%). This best-fit immobile porosity and mass transfer rate of 10^{-5} s^{-1} indicate that the modeled exchange of mass between mobile and immobile domains is negligible, and because the immobile porosity is so small, other mass transfer rates would produce similar breakthrough curves. The similarity of the estimated mass transfer rates for the sand and zeolite are coincidental rather than a product of a similar length scale of mass transfer for the two materials. The rate of mass transfer can be used to calculate a

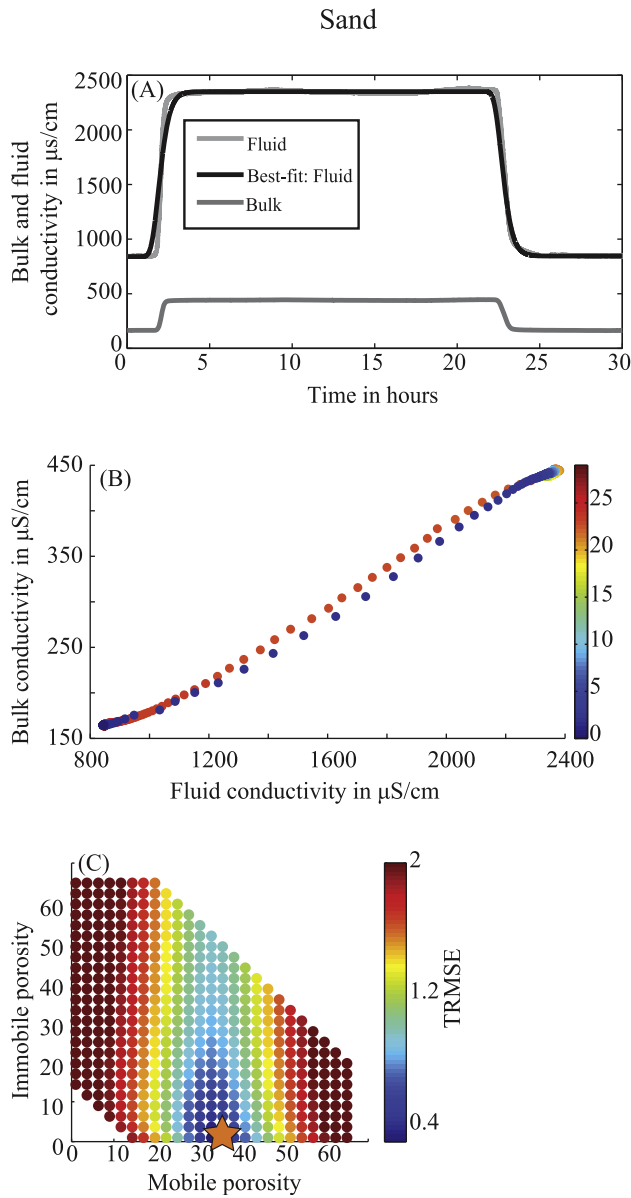


Figure 4. Results from the sand tracer test. (a) The timing of σ_b closely matches σ_f and there is no late-time tailing. (b) Minor hysteresis is observed between σ_f and σ_b . (c) The mobile and immobile porosities are shown for the best-fit mass transfer rate of 10^{-5} s^{-1} . The results for the other mass transfer rates are not shown. The TRMSE does not depend strongly on the immobile porosity because the mass transfer rate is so small that no mass transfer is occurring. Transport behaves like a single domain, advective-dispersive solution. The star shows the best-fit value.

characteristic length scale; however, in this experiment there is little mass transfer occurring, so the mass transfer rate and immobile porosity are likely a fitting parameters rather than representative of the physical system.

4.2. Zeolite

[26] Natural zeolites may contain clays that would make the relation between σ_f and σ_b difficult to interpret because

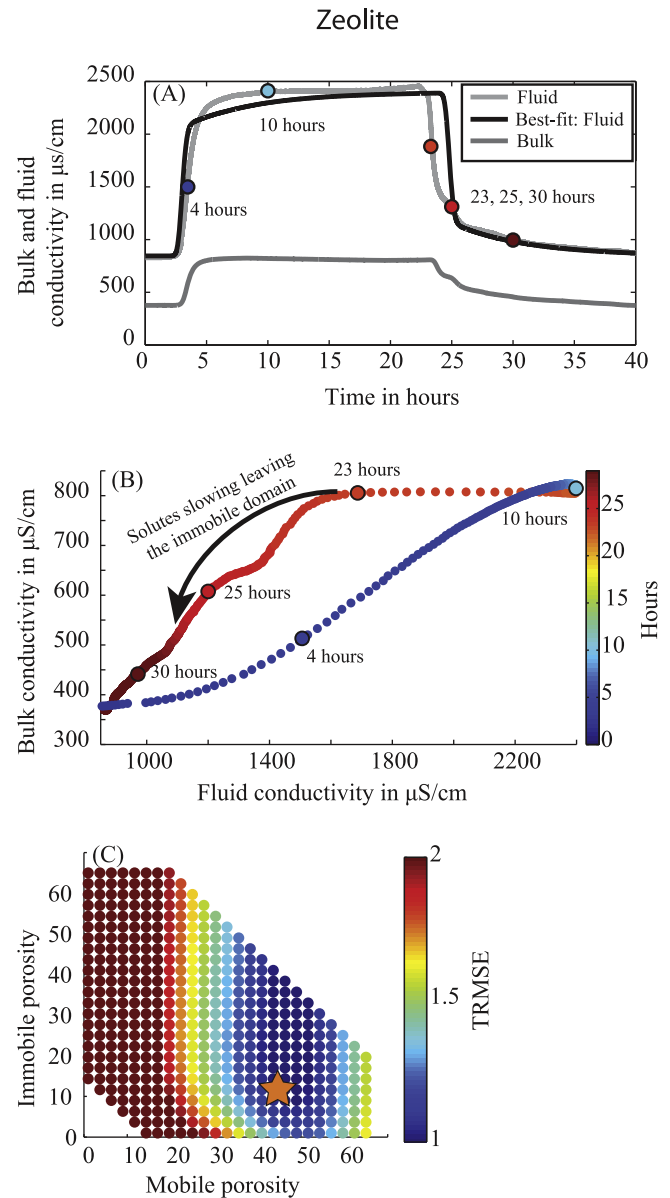


Figure 5. Results from the zeolite tracer test. (a) Tailing is observed, which is better matched by a DDMT model than the ADM. (b) Hysteresis is observed between σ_f and σ_b because solutes are slowly released from the immobile domain. (c) The TRMSE is shown for the immobile and mobile porosities for the best-fit mass transfer rate of 10^{-5} s^{-1} , while the results for the other mass transfer rates are not shown. Changes in the mobile porosity have greater influence on the TRMSE than the immobile porosity. The star shows the best-fit value.

surface conductivity, dependent upon clays and conductance within the electrical double layer, creates a nonlinear relation between σ_b and σ_f [Revil and Glover, 1998]; however, previous analysis of the electrical properties of clinoptilolite shows negligible surface conductivity if clay phases are not present [Revil et al., 2002]. XRD did not indicate the presence of clay phases, so surface conductivity is assumed to contribute negligibly to σ_b .

[27] The zeolite column displays non-Fickian behavior that cannot be explained using the ADM but can be better explained by incorporating first-order rate DDMT. Hysteresis between of σ_f and σ_b is observed for nearly colocated measurements, indicating mass transfer between mobile and immobile domains. Archie's law predicts that the ratio of σ_f and σ_b remains fixed through time. However, in the zeolite tracer test, this ratio varies in time: at early times, σ_b rises more slowly than σ_f , while at late times, σ_b remains elevated relative to σ_f . This lag in time can be attributed to the difference in sampling volumes between σ_f and σ_b , because the point-scale σ_f measurement is restricted to only the mobile domain while σ_b is a bulk average of both the immobile and mobile domains. The slight lag between the σ_f and σ_b observed in the field and numerical modeling experiments has previously been attributed to mass transfer [Day-Lewis and Singha, 2008; Singha et al., 2007], and we can confirm this phenomena here, where no other complicating factors exist. We provide evidence of mass transfer with bypassed pore space and/or slow advection through stagnant or poorly connected pore space, approximated here using what is commonly termed the mobile-immobile framework. Although we consider only a single rate of mass transfer between two domains, we recognize that the DDMT model is a simple approximation of a complicated process that can be more completely described by using a range of residence times or rates.

[28] The best-fit mobile porosity (46%) is similar to the NMR estimate of the mobile porosity (43%); however, the best-fit immobile porosity (20%) is much greater than the NMR estimate of the immobile porosity (7.7%). The TRMSE between observed and modeled σ_f is not as sensitive to the immobile porosity compared to the mobile porosity. As a result of this lower sensitivity, a wide range of estimated immobile porosity values from 12% to 28% result in reasonable approximations of observed solute transport; this lack of sensitivity may explain the overestimate of the immobile and total porosities using this method compared to the NMR-determined immobile porosity. The DDMT model assumes complete mixing between the two domains; incomplete mixing within the mobile and immobile domains may result in overestimation of the immobile pore space. Mass transfer is expected given the DaI of 0.2, based on the best-fit mobile and immobile porosity and mass transfer rate. The total best-fit porosity (66%) is slightly greater than the measured total porosity (54%). The internal porous network of the zeolite serves as a reservoir for water inside the grain itself, resulting in a total porosity greater than expected for a random packing assortment. The SEM images reveal a rough topography and layered sheets, which potentially serve as immobile pore space. The materials studied here were selected to minimize the effects of surface conduction and cation exchange. The zeolite may exhibit cation exchange, but we used a sodium chloride tracer and sodium is the most abundant cation available for exchange; hence the role of cation exchange was minimized.

4.3. Experimental Methods and Limitations

[29] We focus on homogeneously packed, unconsolidated, clay-free material to limit the effect of hydraulic conductivity heterogeneity; consequently, anomalous transport can

be attributed to mass transfer into the immobile domain. Our results show that the comparison of σ_f and σ_b through time can be used to observe the exchange of mass in a DDMT framework, but the scale of these measurements impose practical limits on direct inference of time scales and estimated mass transfer rates, as suggested by Day-Lewis and Singha [2008]. In a multirate environment, a distribution of mass transfer rates and thus DaI numbers exists. Our methods may be sensitive to only an effective mass transfer rate or only those mass transfer rates corresponding to DaI number(s) around unity; future work is needed to investigate the relation between electrical resistivity measurements with multiple rates of mass transfer.

[30] NMR can be used to partition the porosity into mobile and immobile domains, but this method depends on a selected cutoff time. Although the selection of the cutoff time may vary, we use the value of 33 ms used by the petroleum industry for assessing recoverable hydrocarbons in sandstone [Allen et al., 2000; Timur, 1969]. To justify our choice we note that this cutoff time corresponds to an effective pore diameter ranging between 96 and 182 nm, determined from equation (6) using values for the surface relaxivity that represents silica sand ($2.9 \mu\text{m s}^{-1}$) to natural aquifer material ($5.5 \mu\text{m s}^{-1}$) [Hinedi et al., 1997]. This range of pore diameters is in the range expected to differentiate intragrain from intergrain porosity for the zeolite clinoptilolite [Kowalczyk et al., 2006]. We extend this simple assumption to the zeolites, although we stress that this methodology should be taken with caution as a starting point for a future, comprehensive analysis. The T_2 distributions have a large, obvious peak corresponding to mobile domains such that the cutoff time can also be selected from visual inspection. Selecting different cutoff times within an order of magnitude will not dramatically affect the modeled tracer test at late times because the tailing is strongly controlled by the mass transfer rate. Although the NMR results show a pore size distribution, these results cannot reveal any information about the connectivity of these pores. Some pores, large or small, may be entirely disconnected from the rest of the pore network and may be classified as neither mobile nor immobile. Conversely, a fraction of small pores may be strongly connected to the mobile pores. Additionally, small pores with corresponding fast relaxation times may not be detected, resulting in an underestimate of the total porosity. Despite these caveats, the mobile and immobile porosities determined from NMR supports the best-fit modeled parameters.

[31] We stress the importance of complementing concentration samples with electrical geophysics rather than using electrical measurements as a substitute for direct sampling. Although electrical resistivity instruments can automatically and rapidly collect time-lapse information, these methods are limited in their information regarding water chemistry. Similarly, fluid samples are limited by their nature as a point-source measurement consisting primarily of mobile fluids. Each method has unique restrictions that can be minimized when used collectively. Future work can take the findings of this work further by focusing on: (1) the inability to predict the mass transfer rate a priori, (2) the selection of the cutoff time used to partition the total porosity into a mobile and immobile domain with NMR, and (3) the assumption of one mass transfer rate.

5. Conclusions

[32] We present the first controlled, laboratory experimental evidence confirming that the synthesis of σ_f with σ_b can be used to directly estimate properties controlling the operation of mass transfer. The hysteresis between σ_f and σ_b observed in the zeolite tracer test is evidence for the exchange of solutes between immobile and mobile domains, and cannot be explained by large-scale heterogeneity, or by the difference in measurement scales of σ_f and σ_b . In the sand column we did not observe hysteresis between σ_f and σ_b , consistent with advection-dispersion behavior with negligible mass transfer.

[33] We calculated best-fit mass transfer parameters in both sand and zeolite for numerical models with first-order exchange based on σ_f using the Box-Cox transform to emphasize the late-time tailing. The mass transfer rate is the parameter that has the most influence on late-time tailing. For the zeolites we present a best-fit mobile and immobile porosity of 46% and 20%, respectively, and a mass transfer rate of 10^{-5} s^{-1} . These values are similar to our NMR estimates for a mobile and immobile porosity of 43% and 7.7%, respectively. For the sand we present a best-fit mobile and immobile porosity of 33% and 1%, respectively, and a mass transfer rate of 10^{-5} s^{-1} . This is consistent with our NMR estimates for a mobile and immobile porosity of 31% and 0.7%, respectively.

[34] **Acknowledgments.** This research was supported by the Department of Energy Environmental Remediation Science Program grant DE-SC0001773, National Science Foundation Graduate Fellowship DGE-0750756 and DGE-1057607, National Science Foundation grant EAR-0747629, and the U.S. Geological Survey Toxic Substances Hydrology Program. The views and conclusions in this article represent the views solely of the authors and do not necessarily reflect the views of the funding agencies, but do represent the views of the U.S. Geological Survey. Any use of trade, firm, or product names is for descriptive purposes only and does not imply endorsement by the U.S. Government. We thank the reviewers whose comments have led to a significant improvement of this paper.

References

- Adams, E. E., and L. W. Gelhar (1992), Field study of dispersion in a heterogeneous aquifer 2. Spatial moments analysis, *Water Resour. Res.*, 28(12), 3293–3307.
- Allen, D. et al., (2000), Trends in NMR logging, *Oilfield Rev.*, 12(2), 2–19.
- Archie, G. E. (1942), The electrical resistivity log as an aid in determining some reservoir characteristics, *Trans. Am. Inst. Min. Metall. Pet. Eng.*, 146, 54–62, doi:10.2307/777630.
- Arns, C. H. (2004), A comparison of pore size distributions derived by NMR and X-ray-CT techniques, *Phys. A*, 339, 159–165, doi:10.1016/j.physa.2004.03.033.
- Bahr, J. M., and J. Rubin (1987), Direct comparison of kinetic and local equilibrium formulations for solute transport affected by surface reactions, *Water Resour. Res.*, 23(3), 438–452, doi:10.1029/WR023i003.p00438.
- Benson, D. A., S. W. Wheatcraft, and M. M. Meerschaert (2000), Application of a fractional advection-dispersion equation, *Water Resour. Res.*, 36(6), 1403–1412.
- Benson, D. A., R. Schumer, M. M. Meerschaert, and S. W. Wheatcraft (2001), Fractional dispersion, Lévy motion, and the MADE tracer tests, *Transp. Porous Media*, 42, 211–240.
- Berkowitz, B., J. Klafter, R. Metzler, and H. Scher (2002), Physical pictures of transport in heterogeneous media: Advection-dispersion, random-walk, and fractional derivative formulations, *Water Resour. Res.*, 38(10), 1191 doi:10.1029/2001WR001030.
- Berkowitz, B., A. Cortis, M. Dentz, and H. Scher (2006), Modeling non-Fickian transport in geological formations as a continuous time random walk, *Rev. Geophys.*, 44, RG2003, doi:10.1029/2005RG000178.
- Bird, N. R. A., A. R. Preston, E. W. Randall, W. R. Whalley, and A. P. Whitmore (2005), Measurement of the size distribution of water-filled pores at different matric potentials by stray field nuclear magnetic resonance, *Eur. J. Soil Sci.*, 56, 135–143, doi:10.1111/j.1365-2389.2004.00658.x.
- Box, G. E. P., and D. R. Cox (1964), An analysis of transformations, *J. R. Stat. Soc. Ser. B*, 26(2), 211–252.
- Brownstein, K. R., and C. E. Tarr (1979), Importance of classical diffusion in NMR studies of water in biological cells, *Phys. Rev. Sect. A*, 19(6), 2446–2453.
- Carrera, J., X. Sánchez-Vila, I. Benet, A. Medina, G. Galarza, and J. Guimerà (1998), On matrix diffusion: Formulations, solution methods and qualitative effects, *Hydrogeol. J.*, 6(1), 178–190, doi:10.1007/s100400050143.
- Coats, K., and B. Smith (1964), Dead-end pore volume and dispersion in porous media, *J. Sci. Pet. Eng.*, 4(1), 73–84.
- Culkin, S. L., K. Singha, and F. D. Day-Lewis (2008), Implications of rate-limited mass transfer for aquifer storage and recovery, *Ground Water*, 46(4), 517–657, doi:10.1111/j.1745-6584.2008.00435.x.
- Day-Lewis, F. D., and K. Singha (2008), Geoelectrical inference of mass transfer parameters using temporal moments, *Water Resour. Res.*, 44(5), W05201, doi:10.1029/2007WR006750.
- Garré, S., J. Koestel, T. Gunther, M. Javaux, J. Vanderborght, and H. Vereecken (2010), Comparison of heterogeneous transport processes observed with electrical resistivity tomography in two soils, *Vadose Zone J.*, 9(2), 336, doi:10.2136/vzj2009.0086.
- Haggerty, R., and S. M. Gorelick (1995), Multiple-rate mass transfer for modeling diffusion and surface reactions in media with pore-scale heterogeneity, *Water Resour. Res.*, 31(10), 2383–2400, doi:10.1029/95WR10583.
- Haggerty, R., S. A. McKenna, and L. C. Meigs (2000), On the late-time behavior of tracer test breakthrough curves, *Water Resour. Res.*, 36(12), 3467–3479, doi:10.1029/2000WR900214.
- Harvey, C. F., R. Haggerty, and S. M. Gorelick (1994), Aquifer remediation: A method for estimating mass transfer rate coefficients and an evaluation of pulsed pumping, *Water Resour. Res.*, 30(7), 1979–1991, doi:10.1029/94WR00763.
- Hinedi, Z. R., Z. J. Kabala, T. H. Skagg, D. B. Borchardt, R. W. K. Lee, and A. C. Chang (1993), Probing soil and aquifer material porosity with nuclear magnetic resonance, *Water Resour. Res.*, 29(12), 3861–3866, doi:10.1029/93WR02302.
- Hinedi, Z. R., A. C. Chang, M. A. Anderson, and D. B. Borchardt (1997), Quantification of microporosity by nuclear magnetic resonance relaxation of water imbibed in porous media, *Water Resour. Res.* 33(12), 2697–2704.
- Huang, K., N. Toride, and M. T. van Genuchten (1995), Experimental investigation of solute transport in large, homogeneous and heterogeneous, saturated soil columns, *Transp. Porous Media*, 18(3), 283–302, doi:10.1007/BF00616936.
- Keating, K., and R. Knight (2010), A laboratory study of the effect of Fe(II)-bearing minerals on nuclear magnetic resonance (NMR) relaxation measurements, *Geophysics*, 75(3), F71–F82, doi:10.1190/1.3386573.
- Keller, G. V., and F. C. Frischknecht (1966), *Electrical Methods in Geophysical Prospecting*, Pergamon, Oxford, UK.
- Kollat, J. B., P. M. Reed, and T. Wagener (2012), When are multiobjective calibration trade-offs in hydrologic models meaningful?, *Water Resour. Res.*, 48(3), W03520, doi:10.1029/2011WR011534.
- Kowalczyk, P., M. Sprynskyy, A. P. Terzyk, M. Lebedynets, J. Namiećnik, and B. Buszewski (2006), Porous structure of natural and modified clinoptilolites., *J. Colloid Interface Sci.*, 297(1), 77–85, doi:10.1016/j.jcis.2005.10.045.
- Major, E., D. A. Benson, J. Revielle, H. Ibrahim, A. Dean, R. M. Maxwell, E. Poeter, and M. Dogan (2011), Comparison of Fickian and temporally nonlocal transport theories over many scales in an exhaustively sampled sandstone slab, *Water Resour. Res.*, 47(10), W10519, doi:10.1029/2011WR010857.
- Meerschaert, M. M., D. A. Benson, and B. Bäumer (1999), Multidimensional advection and fractional dispersion., *Phys. Rev. E*, 59(5), 5026–5028.
- Misirli, F., H. V. Gupta, S. Sorooshian, and M. Thiemann (2003), *Bayesian Recursive Estimation of Parameter and Output Uncertainty for Watershed Models*, *Water Science Series*, Vol. 6, pp. 113–124, AGU, Washington, D.C.
- Moroni, M., N. Kleinfelder, and J. H. Cushman (2007), Analysis of dispersion in porous media via matched-index particle tracking velocimetry experiments, *Adv. Water Resour.*, 30(1), 1–15, doi:10.1016/j.advwatres.2006.02.005.
- Oliviera, I. B., A. H. Demond, and A. Salehzadeh (1996), Packing of sands for the production of homogeneous porous media, *Soil Sci. Soc. Am. J.*, 60(1), 49–53.

- Reeves, D. M., D. A. Benson, and M. M. Meerschaert (2008), Transport of conservative solutes in simulated fracture networks: 1. Synthetic data generation, *Water Resour. Res.*, *44*, W05404, doi:10.1029/2007WR006069.
- Revil, A., and P. W. J. Glover (1998), Nature of surface electrical conductivity in natural sands, sandstones, and clays, *J. Geophys. Res.*, *25*(5), 691–694.
- Revil, A., D. Hermitte, E. Spangenberg, and J. Cochemé (2002), Electrical properties of zeolitized volcanoclastic materials, *J. Geophys. Res.*, *107*(B8), 2168, doi:10.1029/2001JB000599.
- Senturia, S. D., and J. D. Robinson (1970), Nuclear spin-lattice relaxation of liquids confined in porous solids, *Soc. Pet. Eng. J.*, *10*(3), 237–244.
- Sidle, R. C., B. Nilsson, M. Hansen, and J. Fredericia (1998), Spatially varying hydraulic and solute transport characteristics of a fractured till determined by field tracer tests, Funen, Denmark, *Water Resour. Res.*, *34*(10), 2515–2527.
- Silliman, S. E., L. F. Konikow, and C. I. Voss (1987), Laboratory investigation of longitudinal dispersion in anisotropic porous media, *Water Resour. Res.*, *23*(11), 2145–2151.
- Singha, K., F. D. Day-Lewis, and J. W. Lane, Jr. (2007), Geoelectrical evidence of bicontinuum transport in groundwater, *Geophys. Res. Lett.*, *34*(12), L12401, doi:10.1029/2007GL030019.
- Sprynskyy, M., R. Golembiewski, G. Trykowski, and B. Buszewski (2010), Heterogeneity and hierarchy of clinoptilolite porosity, *J. Phys. Chem. Solids*, *71*(9), 1269–1277, doi:10.1016/j.jpcs.2010.05.006.
- Straley, C., A. Matteson, S. Feng, L. M. Schwartz, W. E. Kenyon, and J. R. Banavar (1987), Magnetic resonance, digital image analysis, and permeability of porous media, *Appl. Phys. Lett.*, *51*(15), 1146–1148.
- Straley, C., D. Roosini, H. J. Vinegar, P. Tutunjian, and C. E. Morriss (1997), Core analysis by low-field NMR, *Log Anal.*, *38*, 84–94.
- Timur, A. (1969), Pulsed nuclear magnetic resonance studies of porosity, movable fluid, and permeability of sandstone, *J. Pet. Technol.*, *21*(6), 755–786.
- Valckenborg, R., L. Pel, and K. Kopinga (2001), Cryoporometry and relaxometry of water in silica-gels, *Magn. Reson. Imaging*, *19*, 489–491.
- van Genuchten, M. T., and P. J. Wierenga (1976), Mass transfer studies in sorbing porous media: I. Analytical solutions, *Soil Sci. Soc. Am. J.*, *40*(4), 473–480.
- van Werkhoven, K., T. Wagener, P. Reed, and Y. Tang (2009), Sensitivity-guided reduction of parametric dimensionality for multi-objective calibration of watershed models, *Adv. Water Resour.*, *32*(8), 1154–1169, doi:10.1016/j.advwatres.2009.03.002.
- Wheaton, D. D., and K. Singha (2010), Investigating the impact of advective and diffusive controls in solute transport on geoelectrical data, *J. Appl. Geophys.*, *72*(1), 10–19, doi:10.1016/j.jappgeo.2010.06.006.
- Whittall, K. P., M. J. Bronskill, and R. M. Henkelman (1991), Investigation of analysis techniques for complicated NMR relaxation data, *J. Magn. Reson.*, *95*(2), 221–234.
- Willmann, M., J. Carrera, and X. Sanchez-Vila (2008), Transport upscaling in heterogeneous aquifers: What physical parameters control memory functions? *Water Resour. Res.*, *44*, W12437, doi:10.1029/2007WR006531.
- Zhang, Y., D. A. Benson, and B. Baeumer (2007), Predicting the tails of breakthrough curves in regional-scale alluvial systems, *Ground Water*, *45*(4), 473–484.
- Zhang, Y., D. A. Benson, and D. M. Reeves (2009), Time and space nonlocalities underlying fractional-derivative models: Distinction and literature review of field applications, *Adv. Water Resour.*, *32*(4), 561–581, doi:10.1016/j.advwatres.2009.0301.0008.